Journal of Alloys and Compounds 825 (2020) 154053

Contents lists available at ScienceDirect

Journal of Alloys and Compounds

journal homepage: http://www.elsevier.com/locate/jalcom

Large magnetic entropy change and refrigeration capacity around room temperature in quinary $Ni_{41}Co_{9-x}Fe_xMn_{40}Sn_{10}$ alloys (x= 2.0 and 2.5)

F. Chen [a, *], J.L. Sánchez Llamazares [b, **], C.F. Sánchez-Valdés [c], Fenghua Chen [d], Zongbin Li [e], Y.X. Tong [a], L. Li [a]

[a] Institute of Materials Processing and Intelligent Manufacturing, College of Materials Science and Chemical Engineering, Harbin Engineering University, Harbin, 150001, China
[b] Instituto Potosino de Investigación Científica y Tecnológica A.C., Camino a la Presa San José 2055, Col. Lomas 4a Sección, San Luis Potosí, S.L.P. 78216, Mexico
[c] División Multidisciplinaria, Ciudad Universitaria, Universidad Autónoma de Ciudad Juárez (UACJ), Calle José de Jesús Macías Delgado # 18100, Ciudad Juárez, Chihuahua, 32579, Mexico
[d] School of Materials Science and Engineering, Taiyuan University of Science and Technology, Taiyuan, 030024, China
[e] Key Laboratory for Anisotropy and Texture of Materials (Ministry of Education), Northeastern University, Shenyang, 110819, China

ARTICLE INFO

Article history:
Received 28 September 2019
Received in revised form
24 January 2020
Accepted 25 January 2020
Available online 28 January 2020

Keywords:
Ni-Co-Mn-Sn Heusler alloys
Iron alloying
Magnetocaloric effect
Magnetic entropy change
Adiabatic temperature change
Refrigeration capacity

ABSTRACT

We report the magnetocaloric properties of two Fe-containing quinary bulk polycrystalline alloys of nominal compositions $Ni_{41}Co_7Fe_2Mn_{40}Sn_{10}$ and $Ni_{41}Co_{6.5}Fe_{2.5}Mn_{40}Sn_{10}$ that were determined by indirect and direct methods. Both samples showed a large refrigeration capacity *RC* and maximum magnetic entropy change ΔS_M^{peak} around room temperature. For a magnetic field change of 2 T (5 T), a large magnetic entropy change of 18.9 (22.4) J kg^{-1} K^{-1} and 11.8 (16.8) J kg^{-1} K^{-1} and a refrigeration capacity of 128 (396) J kg^{-1} and 99 (313) J kg^{-1} were found in $Ni_{41}Co_7Fe_2Mn_{40}Sn_{10}$ and $Ni_{41}Co_{6.5}Fe_{2.5}Mn_{40}Sn_{10}$ alloys, respectively. *RC* for the alloy $Ni_{41}Co_7Fe_2Mn_{40}Sn_{10}$, is among the largest value reported so far for Ni−Mn based Heusler alloys. Under a 1.5 T field change, the direct measurements showed the maximum adiabatic temperature changes ΔT_{ad}^{max} of −0.8 K and −1.5 K for these two alloys, respectively. The present findings point out the potential of Fe-alloyed $Ni_{41}Co_9Mn_{40}Sn_{10}$ Heusler alloys as room-temperature magnetic refrigerants.

1. Introduction

The development of magnetic refrigeration, a new solid-state refrigeration technology that is based on the magnetocaloric effect (MCE), continues to attract considerable attention worldwide due to its environmentally friendly nature, higher energy efficiency, lower mechanical noise and simple mechanical construction, compared with conventional technology based on gas compression/expansion [1–3]. The most important issue for its progress lies on the continuous search of new solid-state magnetic refrigerants that could exhibit a large MCE in an appropriate temperature range as well as the improvement of the existing ones. Up to now hundreds of magnetic refrigeration materials have been synthesized and their magnetocaloric properties were studied, such as pure rare earth elements and their solid solutions [1–4], RE-based compounds [5–14], rare earth-free alloys [15,16], multiphase materials and composites (based on two or more magnetic phases) [17–20], magnetic amorphous and nanocrystalline alloys [21–24], and manganites [21]. Since the discovery of the giant and tunable MCE around room temperature in $Gd_5Ge_2Si_2$ alloys [5,25], other promising alloy systems that favorably combine both properties have been the focus of intensive research. Important families of magnetocaloric materials showing a large first-order MCE around room

* Corresponding author. Institute of Materials Processing and Intelligent Manufacturing College of Materials Science and Chemical Engineering Harbin Engineering University, No.145 Nan Tong Street, Nan-Gang District Harbin, 150001, China.
** Corresponding author. Instituto Potosino de Investigación Científica y Tecnológica A.C., Camino a la Presa San José 2055, Col. Lomas 4ª sección, San Luis Potosí, S.L.P, 78216, Mexico.
E-mail addresses: chenfeng01@hrbeu.edu.cn (F. Chen), jose.sanchez@ipicyt.edu.mx (J.L. Sánchez Llamazares).

https://doi.org/10.1016/j.jallcom.2020.154053
0925-8388/

temperature are La(Fe, Si)$_{13}$-based alloys [21,26,28], (Mn,Fe)$_2$P-type alloys [21,26,27], MnTX-based alloys (T = Ni, Co, Fe; X = Ge, Si) [29–33], and Heusler-type Ni–Mn-Z (Z: group IIIA-VA elements) alloys (with or without Co) [34–48]. Their large, and in some cases giant, MCE comes from the magnetostructural coupling (i.e., the strong coupling between the structural and magnetic transitions [1–3]).

Among Ni–Mn-Z (Z = In, Sn, Ga and Sb) Heusler alloys, the large maximum magnetic entropy change ΔS_M^{peak} [37,38,49–55], easily adjustable working temperature [56], low cost [57] and non-toxicity of raw materials [57] make Ni–Mn–Sn alloys promising candidates for their utilization as working substances in commercial cooling devices. However, brittleness and considerable magnetic field-induced hysteresis loss *HL*, still hinder their practical applications. In a recent work, it was shown that Fe substitution for Co, equal to or more than 2 at. %, was effective in reducing the brittleness and magnetic field-induced hysteresis loss in the bulk $Ni_{41}Co_9Mn_{40}Sn_{10}$ alloy [58]. To go deeper into the potential use of these Fe-containing quinary alloys as magnetic refrigerants, a more complete characterization of their magneto caloric properties must be conducted. With such a purpose, two bulk quinary alloys that had a nominal composition of $Ni_{41}Co_7Fe_2Mn_{40}Sn_{10}$ and $Ni_{41}Co_{6.5}Fe_{2.5}Mn_{40}Sn_{10}$ were prepared, and their magnetocaloric properties were determined by both indirect (the determination of the magnetic entropy change curves from isothermal magnetization measurements) and direct (the measurement of the adiabatic temperature change) methods. Finally, the alloys that had a higher at. % content of Fe were not considered because the magnitude of ΔS_M^{peak} became considerably reduced [58].

2. Experimental procedure

Bulk polycrystalline alloys with nominal compositions of $Ni_{41}Co_7Fe_2Mn_{40}Sn_{10}$ and $Ni_{41}Co_{6.5}Fe_{2.5}Mn_{40}Sn_{10}$ were produced by arc melting from high-purity elements (≥99.9%). They will be referred hereafter as Fe_2 and $Fe_{2.5}$, respectively. The ingots were flipped and melted several times to reach a good starting chemical homogeneity. For a definitive homogenization, a thermal annealing was performed under vacuum at 1173 K for 6 h; in which the process ended with a water quenching.

The microstructure and elemental chemical composition of samples were examined in a FEI Quanta 250 scanning electron microscope (SEM), which was equipped with an energy dispersive X-ray spectroscopy (EDS) system. After three EDS analyses were taken in different regions of the matrix for the thermally annealed samples, the average elemental chemical composition of Fe_2 and $Fe_{2.5}$ alloys were $Ni_{38.9}Co_{6.6}Fe_{1.9}Mn_{43.5}Sn_{9.1}$ and $Ni_{38.6}Co_{6.1}Fe_{2.7}Mn_{43.5}Sn_{9.3}$, respectively. The structural phase transformation was studied by a differential scanning calorimetry (DSC) using the PerkinElmer Diamond DSC system where the heating/cooling rate was 10 K/min.

Magnetization measurements were carried out with the vibrating sample magnetometer option fitted to a 9 T Quantum Design PPMS® Dynacool® system. Samples with the approximate dimensions of 0.4 × 0.4 × 3.0 mm^3 were prepared for magnetic measurements. The magnetic field $\mu_o H$ was applied along the major length of these parallelepiped-shaped samples in order to minimize the internal demagnetizing field. Due to the strong effect of the magnetic field on the reverse martensitic phase transition, a fixed thermal protocol, referred elsewhere as back and forward [59], was followed prior to the measurement of each isothermal magnetization $M(\mu_o H)$ curve in the phase transition T region. At zero magnetic field the sample was heated to 400 K to stabilize austenite, cooled to 300 K to completely form martensite, and then heated again in no-overshoot mode to the selected measuring temperature T_{meas}. This procedure ensures that before the magnetic field is applied the sample exhibits the phase constitution that corresponds to the thermally induced structural transition.

A self-designed experimental setup was used to perform direct measurements of the adiabatic temperature variation (ΔT_{ad}) under a magnetic field change of 1.5 T. For this measurement, rectangular parallelepiped samples with the approximate dimensions of 5 × 5 × 10 mm^3 were used. A NdFeB permanent magnet Halbach array produced the applied magnetic field along the longer direction of the sample whereas its temperature change was measured by a thermocouple in intimate contact. The magnetization and demagnetization conditions were carried out by inserting and extracting the sample into the uniform magnetic field region that was created with a Halbach array. For these reasons, the above operations ensure a near-adiabatic condition.

3. Experimental results and discussion

Fig. 1 shows a room temperature SEM image of the $Fe_{2.5}$ sample (293 K). The small dark particles with irregular morphology appearing in the intra and intergranular regions have been identified as γ phase [53,58]. This suggests that Fe addition favors the formation of the γ phase, as observed in $Ni_{50}Mn_{34}In_{16-y}Fe_y$ (y > 5) [60], $Ni_{50.5}Mn_{25-x}Fe_xGa_{24.5}$ (x > 17) [61], and $Ni_{50}Mn_{40-x}Sn_{10}Fe_x$ (x > 3) alloys [62]. The amount of γ phase particles increases from Fe_2 (as reported in our recent work [58]) to $Fe_{2.5}$. This phase reduces the amount of the matrix phase with the consequent adverse effect on the maximum magnetic entropy change ΔS_M^{peak} [53,58,63], as described below. In the $Fe_{2.5}$ sample, there was no evidence of the martensite phase due to the martensitic transition temperature was below 293 K and lower than that of Fe_2 as well, as inferred from the DSC curves presented below.

Fig. 2 displays DSC curves and low-field (5 mT) and high-field (5 T) magnetization as a function of temperature, $M(T)$, curves measured in both zero-field-cooled (ZFC) and field-cooled (FC) modes for the Fe_2 and $Fe_{2.5}$ samples, respectively. The $M(T)$ curves were measured at a heating/cooling rate of 1.0 Kmin^{-1}. The starting and finishing phase transformation temperatures determined from the $M(T)^{5mT}$ and DSC curves were in good agreement. By applying the conventional tangent extrapolation method to the $M(T)^{5mT}$ curve, the starting (A_S) and finishing (A_f) temperatures for the reverse martensitic transition, and the starting (M_S) and finishing (M_f) temperatures for the martensitic transformation were determined. For the Fe_2 sample, A_S = 293 K, A_f = 303 K, M_S = 287 K, and M_f = 277 K. Upon the application of a 5 T field (Fig. 2(c)) these temperatures reduced to: A_S^{5T} = 270 K, A_f^{5T} = 290 K, M_S^{5T} = 263 K,

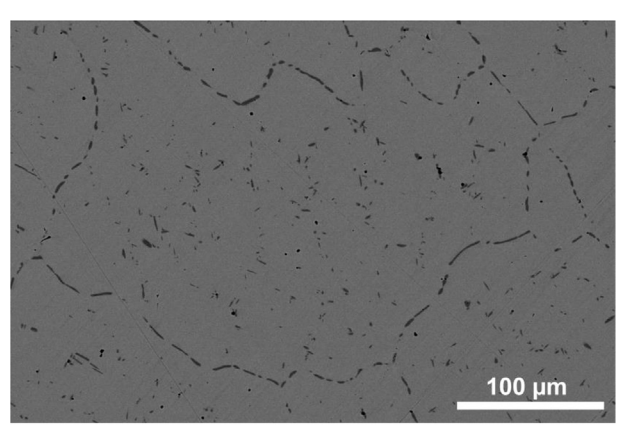

Fig. 1. Surface microstructure observed by SEM for the $Fe_{2.5}$ sample.

and $M_f^{5T} = 244$ K. This magnetic field-induced temperature shift of the structural transition temperatures is a well-known common feature of (Ni–Mn-Z)-based metamagnetic shape memory alloys (Z = In, Sn and Sb). The ratio between transformation temperature change and magnetic field change ($\Delta T/\mu_o\Delta H$) can be obtained when referring to the equilibrium temperature of the reverse martensitic transformation, T_A, as determined from dM/dT vs. T curve upon heating shown at the inset of Fig. 2(c). For this sample, T_A is reduced from 300 to 279 K when the magnetic field is increased from 5 mT to 5 T (i.e., 21 K) giving rise to $\Delta T_A/\mu_o\Delta H = 4.2$ K/T. This large field dependence of transformation temperatures ratio is comparable to the reported for $Ni_{45}Co_5Mn_{36.6}In_{13.4}$ ($\Delta T/\mu_o\Delta H = 4.3$ K/T) [64], and larger than that of $Ni_{43}Co_7Mn_{39}Sn_{11}$ ($\Delta T/\mu_o\Delta H = 3.6$ K/T) [65]. According to the Clausius-Clapeyron relation [64], $\Delta T_A/\mu_o\Delta H = \Delta M_{A\text{-}M}/\Delta S_{tr}$ where $\Delta M_{A\text{-}M}$ is the magnetization difference between the austenite and martensite phase. As for this sample $\Delta M_{A\text{-}M} = 88.2$ $Am^2\ kg^{-1}$ at $\mu_oH = 5$ T, the estimated ΔS_{tr} associated with the reverse martensitic transformation was 21.0 J kg^{-1} K^{-1}. A large value of ΔS_{tr} means a large magnetic entropy change provided that the applied magnetic field induces the complete reverse martensitic transformation [55,56,66,67], therefore a large ΔS_M^{peak} was attained for the present alloy. Besides, the temperature range of the reverse martensitic transformation (A_f - A_S) was extended from 10 K at 5 mT to 20 K when the applied magnetic field increased up to 5 T. Hence, the application of magnetic field not only decreased the structural transition temperatures, but also widened the transformation interval as a prerequisite for the attainment of a large refrigerant capacity.

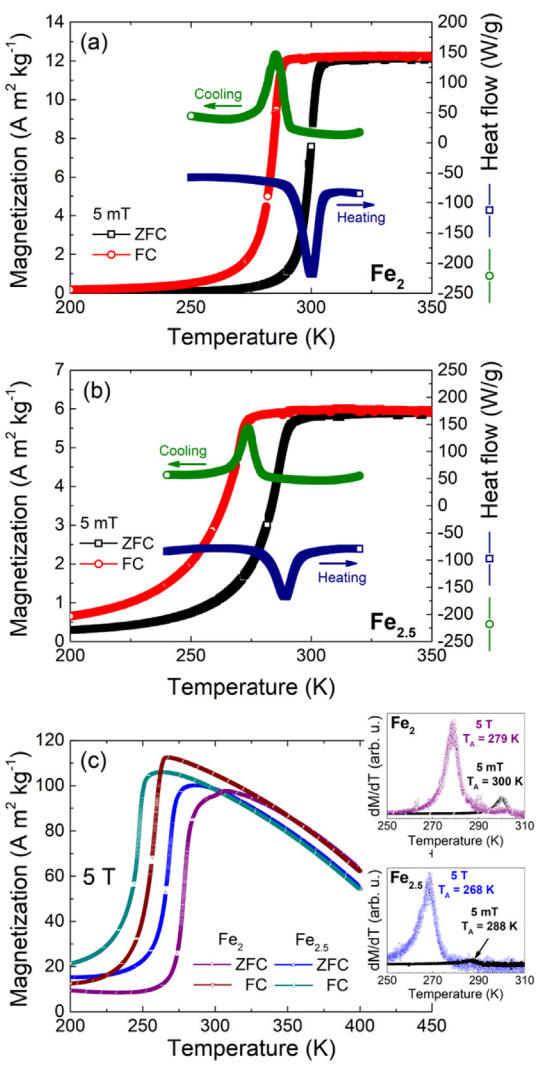

Fig. 2. DSC curves and temperature dependence of magnetization under a static magnetic field of 5 mT following ZFC and FC protocols: (a) Fe_2 sample, and (b) $Fe_{2.5}$ sample. (c) $M(T)$ curves under 5 T field measured in ZFC and FC modes for both samples. Inset: dM/dT vs. T curve upon heating at 5 mT and 5 T.

As determined from Fig. 2(b), for the $Fe_{2.5}$ sample, $A_S = 276$ K, $A_f = 291$ K, $M_S = 272$ K, and $M_f = 253$ K. Hence, at room temperature almost all the martensite had transformed into austenite, in good agreement with SEM observations (Fig. 1). Besides, the decrease of transformation temperatures that were caused by the increase of Fe substitution for Co proved the effectiveness of Fe alloying in adjusting structural transformation temperatures, which agreed with other reports related to Fe-containing Ni–Mn–Sn based alloys [37,58,62,68–70]. The martensitic transformation temperature usually decreases with the Fe content when Fe replaces Ni, Mn, or Co in these Ni–Mn–Sn based alloys either due to the variation of the valence electron concentrations per atom e/a [37] or the formation of the second phase [70]. Upon the application of a 5 T magnetic field, $A_S{}^{5T} = 250$ K, $A_f{}^{5T} = 275$ K, $M_s{}^{5T} = 254$ K, and $M_f{}^{5T} = 223$ K whereas T_A was reduced from 288 to 268 K (as the inset of Fig. 2(c) shows). Accordingly, $\Delta T_A/\mu_o\Delta H$ was 4.0 K/T, which is smaller than the one of the Fe_2 sample, and $\Delta M_{A\text{-}M}$ at 5 T is 81.2 $Am^2\ kg^{-1}$. So, ΔS_{tr} was calculated to be 20.3 J kg^{-1} K^{-1}, that means a large ΔS_M^{peak} must be also expected, although it is slightly smaller than that of the Fe_2 sample. Besides, the temperature range of the reverse martensitic transformation ($A_f - A_S$) was extended from 15 K at 5 mT to 25 K when the applied magnetic field increased up to 5 T. Hence, just like in the Fe_2 sample, a giant refrigeration capacity can be anticipated.

Notably, increasing the substitution of Co by Fe reduces $\Delta M_{A\text{-}M}$ at 5 T from 88.2 A m^2 kg^{-1} for Fe_2 to 81.2 A m^2 kg^{-1} for $Fe_{2.5}$ alloys. This indirectly confirms that the incorporation of Co to Ni–Mn–Sn enhances the magnetization change across the martensitic transformation, as reported in Refs. [38,71,72]; the enhancement is obviously higher than the one which was obtained with Fe alloying [73]. The decrease of $\Delta M_{A\text{-}M}$ led to the reduction of Zeeman energy $\mu_o\Delta M_{A\text{-}M}\cdot H$ and hence reduced the driving force to induce the reverse martensitic transformation [74]. Accordingly, the shift of martensitic transformation temperatures caused by the same external magnetic field in $Fe_{2.5}$ was smaller than that in Fe_2. In addition, the influence of $\Delta M_{A\text{-}M}$ on the magnetic entropy changes should not be neglected, as will be discussed below.

Fig. 3(a) and (b) show the isothermal magnetization versus the magnetic field $M(\mu_oH)$ curves through the reverse martensitic transformation for both alloys (the temperature step between two successive isotherms is 0.5 K). Within a specific temperature range (274 K ~ 295 K for Fe_2, and 262 K ~ 284.5 K for $Fe_{2.5}$), the $M(\mu_oH)$ curves exhibit the characteristically metamagnetic-like behavior. That is, with the increase of the field, the magnetization initially tends to show a ferromagnetic-like behavior followed by a sudden increase in the dM/dH slope above a certain critical field value, μ_oH_{cr} (e.g., $\mu_oH_{cr} \cong 2.5$ T at 272.5 K estimated by the tangent method as shown in Fig. 3(b)) due to the magnetic-field induced reverse martensitic transformation. This metamagnetic feature, which was firstly reported in $Ni_{50}Mn_{36}Sn_{14}$ [75] and $Ni_{45}Co_5Mn_{36.7}In_{13.3}$ [64], is typical of Ni–Mn-Z Heusler alloys [56,57,65,76–78], and substantially contributes to their giant MCE across the reverse martensitic transformation [45]. Therefore, for both Fe_2 and $Fe_{2.5}$ samples, μ_oH_{cr} gradually decreased with increasing measuring temperature. The closer the measuring temperature is to A_f, the lower the value of μ_oH_{cr} is. As known, when the temperature approaches to the A_f, the fraction of the remaining martensite becomes smaller, as a result the magnetic field that was

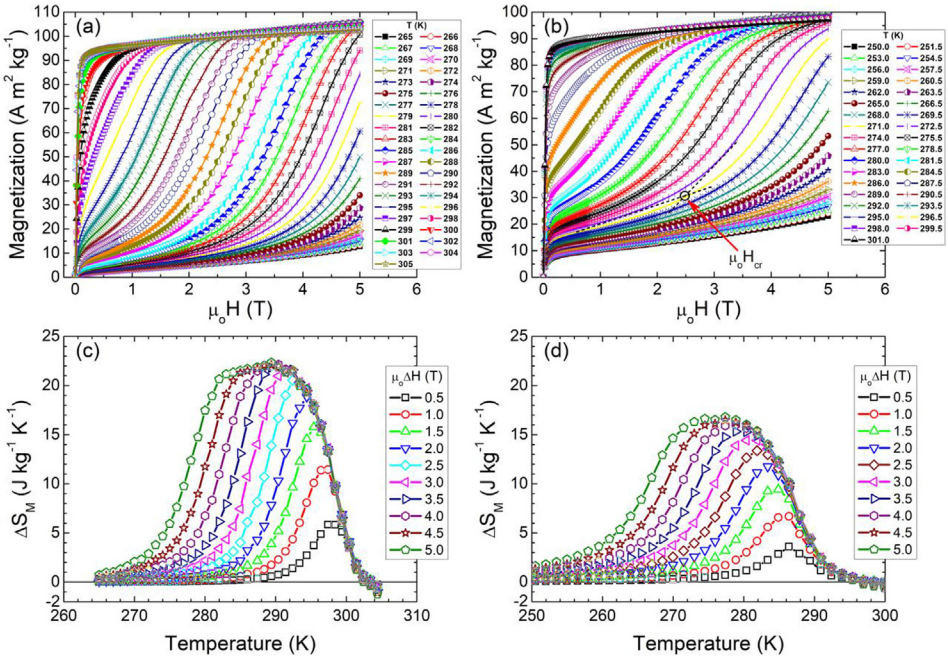

Fig. 3. Isothermal magnetization curves [(a) and (b)] and $\Delta S_M(T)$ curves for selected $\mu_o\Delta H$ values [(c) and (d)] for Fe_2 and $Fe_{2.5}$ samples, respectively.

required to induce the transformation from the martensite to austenite also gets smaller.

The magnetic entropy change ΔS_M is one of the relevant parameters that physically describes the magnetocaloric response of a given material, and its thermal dependence in the phase transition region can be indirectly estimated from a set of $M(\mu_o H)$ curves through the Maxwell relation (i.e., $\Delta S_M(T, \mu_\circ \Delta H) = \mu_\circ \int_0^{\mu_\circ H_{max}} \left[\frac{\partial M(T,\mu_\circ H')}{\partial T}\right]_{\mu_\circ H'} dH'$).

The $\Delta S_M(T)$ curves for ten selected $\mu_o\Delta H$ values are given in Fig. 3(c) and (d) for Fe_2 and $Fe_{2.5}$ alloys, respectively. The maximum value of entropy change ΔS_M^{peak} was 22.4 J kg^{-1} K^{-1} for Fe_2 being larger than 16.8 J kg^{-1} K^{-1} obtained for $Fe_{2.5}$. However, both alloys show a large magnetic entropy change near room temperature. The former is very close and the latter is smaller in comparison with the entropy change ΔS_{tr} estimated above using the Clausius-Clapeyron relation. In addition, the ΔS_{tr} values, determined directly from the DSC curves in Fig. 2, were 22.5 and 19.4 J kg^{-1} K^{-1} for Fe_2 and $Fe_{2.5}$ samples, respectively. The difference between them and the ones calculated from the Clausius-Clapeyron relation, namely 21.0 and 20.3 J kg^{-1} K^{-1}, are quite close. The comparison of the entropy change indirectly estimated from the Maxwell relation and Clausius-Clapeyron relation, and the ones that were directly obtained from the DSC measurement shows that the magnetic entropy change is limited by ΔS_{tr}. Hence, ΔS_{tr} is deciding the maximum value of ΔS_M across the first-order magnetostructural transition for these Ni–Mn-based Heulser alloys. A similar conclusion has been also pointed out in Refs. [55,56,66,67]. As known that, the entropy of each phase is determined by their crystal structure, this means that, for a Ni–Mn-based alloy with a specific composition, the austenite and martensite phases have different values of entropy. Nevertheless, the entropy change is constant during the structural transition which is the ΔS_{tr} directly measured by the DSC. The magnetic field cannot change the structure of each phase, instead it only induces the transition from the martensite to the austenite phase. Therefore, if a magnetic field is large enough to completely induce the structural transition the maximum ΔS_M equals to ΔS_{tr}. This may provide a feasible way to determine the maximum value of ΔS_M in Ni–Mn-based Heulser alloys, that is, by directly measuring ΔS_{tr} using the DSC under zero magnetic field. This method is easier and cheaper in comparison with the indirect methods. However, it should be noted that with this method we can just determine the maximum entropy change. For additional information such as the determination of the shape of the $\Delta S_M(T)$ curve, the dependence of maximum magnetic entropy change on the magnetic field change or other parameters related to $\Delta S_M(T)$, such as *RC*, the indirect methods have to be used.

Besides, the $\Delta S_M(T)$ curves showed a wide "hump-like" peak above 3 T for Fe_2 and 4 T for $Fe_{2.5}$. Particularly in Fe_2, a broad plateau with ΔS_M of about 20 J kg^{-1} K^{-1} occurred over a temperature range from 282 K to 292 K under a 5 T field change. The variation of ΔS_M^{peak} between the present two samples may be due to the fact that the substitution of Co by Fe decreases $\Delta M_{A\text{-}M}$ from 88.2 A m^2 kg^{-1} to 81.2 A m^2 kg^{-1} whereas the temperature range of the reverse martensitic transformation (ΔT) increases from 10 K to 15 K. Indeed, these two reasons could be readily understood from the Maxwell relation itself, because ΔS_M is directly proportional to the first derivative of magnetization with respect to the temperature. In addition, a larger amount of the second γ phase forms with the increase of Fe content. This phase does not participate in the martensitic transformation with the consequent decrease of ΔS_M^{peak}, as confirmed in Refs. [53,58].

The working temperature range δT_{FWHM} was assessed through the full-width at half-maximum of the $\Delta S_M(T)$ curve, i.e., $\delta T_{FWHM} = T_{hot} - T_{cold}$ where T_{hot} and T_{cold} are the temperatures at which ΔS_M is half of its maximum value. The obtained δT_{FWHM}, T_{hot} and T_{cold} are listed in Tables 1 and 2. Under 5 T field, for Fe_2, T_{hot} and T_{cold} are 298 and 278 K, respectively. For $Fe_{2.5}$, they are 287 and 265 K, respectively. For both samples, the working temperature ranges are located around room temperature.

Fig. 4 displays ΔS_M^{eak} as a function of $\mu_o\Delta H$ for Fe_2 and $Fe_{2.5}$, respectively. In spite of the different values of ΔS_M^{peak} the trend of the curves is similar for both samples: the maximum entropy change ΔS_M^{peak} first increases and then tends to saturate with the increase of the magnetic field change above approximately 3 T for

Table 1
Magnetocaloric properties derived from the $\Delta S_M(T)$ curve for Fe_2 alloy for selected magnetic field changes ranging from 1 T to 5 T.

$\mu_o\Delta H$ (T)	1.0	2.0	3.0	4.0	5.0
ΔS_M^{peak} (J kg^{-1} K^{-1})	11.4	18.9	21.3	22.2	22.4
RC (J kg^{-1})	60	128	216	302	396
δT_{FWHM} (K)	7	9	12	16	20
T_{hot} (K)	300	299	298	298	298
T_{cold} (K)	293	290	286	282	278

Table 2
Magnetocaloric properties derived from the $\Delta S_M(T)$ curve for $Fe_{2.5}$ alloy for selected magnetic field changes ranging from 1 T to 5 T.

$\mu_o\Delta H$ (T)	1.0	2.0	3.0	4.0	5.0
ΔS_M^{peak} (J kg^{-1} K^{-1})	6.7	11.8	14.4	16.0	16.8
RC (J kg^{-1})	45	99	164	236	313
δT_{FWHM} (K)	8	10	13	17	22
T_{hot} (K)	289	288	287	287	287
T_{cold} (K)	281	278	274	270	265

Fe_2 and 4 T for $Fe_{2.5}$, in good agreement with those magnetic fields above which a wide "hump-like" peak starts to occur. For the sake of comparison, the ΔS_M^{peak} values of some studied Ni–Mn–Sn magnetocaloric alloys with transitions around room temperature (i.e., from 280 to 316 K) were plotted in Fig. 4. It is clear that, for Fe_2 the values of ΔS_M^{peak} under various magnetic fields are comparable to, or even larger, than most of Ni–Mn–Sn alloys. The ΔS_M^{peak} values and related parameters of the present two alloys for selected $\mu_o\Delta H$ values are given in Tables 1 and 2

Refrigeration capacity RC, which is a physical quantity that quantifies the amount of heat that might be transferred between the cold and hot reservoirs through an ideal refrigeration cycle, is another important parameter that characterizes magnetocaloric materials [1,79,80]. RC can be estimated as $RC = \int_{T_{cold}}^{T_{hot}} \Delta S_M dT$ [79]. The dependence of RC on $\mu_o\Delta H$ of the present alloys is depicted in Fig. 5, and the obtained values for different magnetic field changes are listed in Tables 1 and 2 As Fig. 5 shows, RC monotonically increased with increasing magnetic field changes for both alloys. For $\mu_o\Delta H = 5$ T, the RC value of Fe_2 not taking into consideration the magnetic hysteresis losses is 396 J kg^{-1}, which is a little smaller than that in $Ni_{40}Co_{10}Mn_{40}Sn_{10}$ (426 J kg^{-1}) possessing the largest

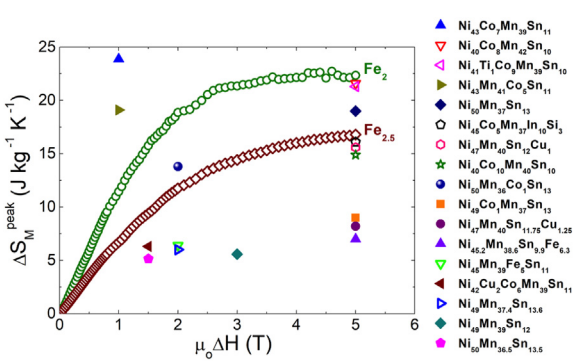

Fig. 4. ΔS_M^{peak} as a function of $\mu_o\Delta H$ for Fe_2 and $Fe_{2.5}$ samples. For the sake of comparison, the ΔS_M^{peak} reported for some studied Ni–Mn–Sn based bulk alloys, with ΔS_M^{peak} between 280 and 316 K, is given. The composition of the selected alloys is listed in the descend order of ΔS_M^{peak} value: $Ni_{43}Co_7Mn_{39}Sn_{11}$ ribbon [54], $Ni_{40}Co_8Mn_{42}Sn_{10}$ [77], $Ni_{41}Ti_1Co_9Mn_{39}Sn_{10}$ [56], $Ni_{43}Mn_{41}Co_5Sn_{11}$ [38], $Ni_{50}Mn_{37}Sn_{13}$ [34], $Ni_{45}Co_5Mn_{37}In_{10}Si_3$ [94], $Ni_{47}Mn_{40}Sn_{12}Cu_1$ [82], $Ni_{40}Co_{10}Mn_{40}Sn_{10}$ [52], $Ni_{50}Mn_{36}Co_1Sn_{13}$ [36], $Ni_{49}Co_1Mn_{37}Sn_{13}$ [37], $Ni_{47}Mn_{40}Sn_{11.75}Cu_{1.25}$ [82], $Ni_{45.2}Mn_{38.6}Sn_{9.9}Fe_{6.3}$ [69], **$Ni_{45}(Mn_{39}Fe_5)Sn_{11}$** [95], $Ni_{42}Cu_2Co_6Mn_{39}Sn_{11}$ [96], $Ni_{49}Mn_{37.4}Sn_{13.6}$ [35], $Ni_{49}Mn_{39}Sn_{12}$ [81], and $Ni_{50}Mn_{36.5}Sn_{13.5}$ [97].

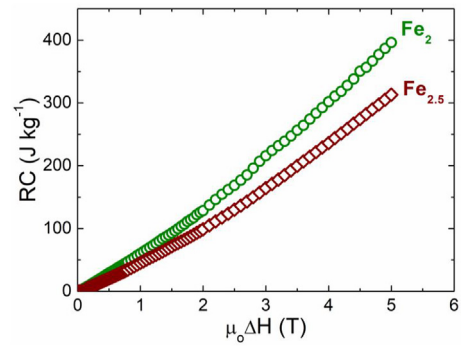

Fig. 5. Refrigeration capacity as a function of the magnetic field change for Fe_2 and $Fe_{2.5}$ samples.

RC reported in Ni–Mn-Z Heusler alloys before the year of 2014 [52]. The RC values of those Ni–Mn-Z alloys that have been reported since 2014 up to now are listed in Table 3. It can be seen that, except for $Ni_{40}Co_8Mn_{42}Sn_{10}$ ($RC = 468$ J kg^{-1}) [77] and $Ni_{42}Co_8Mn_{37.7}In_{12.3}$ ($RC = 450$ J kg^{-1}) [78], the current obtained value is larger than the reported for other Ni–Mn-Z alloys. $Fe_{2.5}$ has a relatively smaller value of RC (313 J kg^{-1}) than Fe_2 resulting from the reduced ΔS_M^{peak} (16.8 J kg^{-1} K^{-1}) and slightly increased δT_{FWHM} (22 K). The large RC values of both alloys are consistent with their large ΔS_M^{peak} (22.4 and 16.8 J kg^{-1} K^{-1}) and broad $\Delta S_M(T)$ curves ($\delta T_{FWHM} = 20$ and 22 K).

As the magnetic field-induced hysteresis loss is inevitable, the effective RC, which is usually referred as RC_{eff}, is more important from the viewpoint of practical application. For a magnetic field of 2 T (the maximum field that commercial permanent magnet assemblies used in magnetic refrigerators prototypes could provide), the average hysteresis loss <HL> value obtained for Fe_2 and $Fe_{2.5}$ alloys in the temperature interval δT_{FWHM} was 43 and 32 J kg^{-1}, respectively, that led to RC_{eff} values of 85 and 67 J kg^{-1}. That is, across the first-order phase transition, the refrigerant capacity would be reduced approximately 33% for both alloys if an ideal refrigeration cycle was considered. In spite of the considerable hysteresis loss, RC_{eff} for Fe_2 samples was still higher than the measured for other Ni–Mn-Z alloys such as $Ni_{49}Mn_{39}Sn_{12}$ ($RC_{eff} = 58$ J kg^{-1} for $\mu_o\Delta H = 3$ T) [81], $Ni_{47}Mn_{40}Sn_{13}$ ($RC_{eff} = 62$ J kg^{-1} for $\mu_o\Delta H = 5$ T) [82], $Ni_{50}Mn_{37}Sn_{13}$ ($RC_{eff} = 54$ J kg^{-1} for $\mu_o\Delta H = 5$ T) [83], and $Ni_{49.8}Co_{1.2}Mn_{33.3}In_{15.5}$ ($RC_{eff} = 76.6$ J kg^{-1} for $\mu_o\Delta H = 5$ T) [84]. Besides, it can be also found that the increase of Fe content reduces the hysteresis loss.

To further explore the potential of the present alloys as magnetocaloric refrigerants, it is worth performing the direct

Table 3
Comparison of the RC values at 5 T obtained for Fe_2 and $Fe_{2.5}$ alloys with those reported since 2014 for some representative Ni–Mn-Z alloys.

Alloy composition	$\mu_o\Delta H$ (T)	RC (J kg^{-1})	Refs.
$Ni_{40}Co_8Mn_{42}Sn_{10}$	5	468	[77]
$Ni_{42}Co_8Mn_{37.7}In_{12.3}$	5	450	[78]
$Ni_{41}Co_7Fe_2Mn_{40}Sn_{10}$	5	396	This work
$Ni_{42}Co_8Mn_{38}In_{12}$	5	334	[86]
Ni_{41} Mn_{43} $Sn_{10}Co_6$	5	322	[87]
$Ni_{41}Co_{6.5}Fe_{2.5}Mn_{40}Sn_{10}$	5	313	This work
$Ni_{48.4}Co_{34.2}Mn_{34.2}In_{13.8}Ga_{1.7}$	5	312	[88]
$Ni_{40.6}Co_{8.5}Mn_{40.9}Sn_{10}$	5	302	[76]
$Ni_{40}Co_{10}Mn_{40}Sn_{10}$ annealed powders	5	279	[89]
$Ni_{45.8}Fe_{4.2}Mn_{38.0}Sn_{12.0}$	5	237	[90]
$Ni_{43}Mn_{46}Sn_{11}C_2$	5	220	[91]
$Ni_{47}Mn_{40}Sn_{13}$	5	207	[82]
Ni_2MnIn	5	167.5	[92]
$Ni_{50}Mn_{35}In_{13.9}B_{1.1}$	5	140	[93]

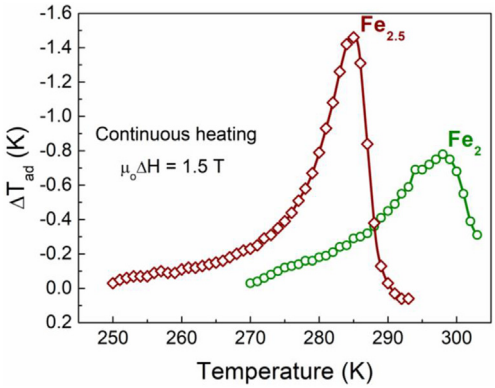

Fig. 6. Adiabatic temperature change (ΔT_{ad}) measured on continuous heating protocol for an external magnetic field change of 1.5 T.

measurement of the adiabatic temperature change ΔT_{ad}. The obtained ΔT_{ad} as a function temperature measured under an external field change of 1.5 T is shown in Fig. 6. Each measurement was performed in continuous heating mode, i.e., the sample was firstly cooled down to 270 K (Fe_2) and 250 K ($Fe_{2.5}$) under zero field to ensure full martensite and then heated to the first measurement temperature under zero field. After finishing the ΔT_{ad} measurement, the sample was heated to the next temperature to perform a subsequent measurement. The maximum ΔT_{ad}^{peak} obtained was −0.8 K at 298 K for Fe_2 and −1.5 K at 285 K for $Fe_{2.5}$. If it is true that the absolute ΔT_{ad}^{peak} values obtained for the studied alloys are not very large compared to the reported for $Ni_{40}Co_8Mn_{42}Sn_{10}$ (4.4 K for $\mu_o\Delta H = 1.5$ T) [77], they favorably compare with the values reported for other Ni−Mn−Sn based alloys such as $Ni_{50}Co_1Mn_{36}Sn_{13}$ (1.1 K for $\mu_o\Delta H = 1.9$ T) [36], $Ni_{46.2}Mn_{36.6}Sn_{12.2}Co_{5.0}$ (1.4 K for $\mu_o\Delta H = 1.9$ T) and $Ni_{51.2}Mn_{35.1}Sn_{13.7}$ (1.1 K for $\mu_o\Delta H = 1.9$ T) [85]. It should be pointed out that, the present ΔT_{ad} values were attained at $\mu_o\Delta H = 1.5$ T, a field unable to fully induce the reverse martensitic transformation (as can be seen from Fig. 3). Secondly, the measurements of ΔT_{ad} were done in the continuous heating mode, which results in an underestimation on the values [77]. Therefore, the actual ΔT_{ad} for the present alloys should be somewhat larger than the measured one.

4. Conclusions

In summary, the magnetocaloric properties of two bulk quinary alloys of nominal composition of $Ni_{41}Co_7Fe_2Mn_{40}Sn_{10}$ and $Ni_{41}Co_{6.5}Fe_{2.5}Mn_{40}Sn_{10}$ were studied by indirect and direct methods. For a magnetic field change of 2 T (5 T), both alloys exhibited a large maximum magnetic entropy change around room temperature of 18.9 (22.4) J kg^{-1} K^{-1} and 11.8 (16.8) J kg^{-1} K^{-1}, respectively, giant refrigeration capacity values of 128 (396) J kg^{-1} and 99 (313) J kg^{-1} and a widened working temperature range δT_{FWHM}. A direct measurement of adiabatic temperature changes showed ΔT_{ad}^{peak} values of −0.8 K and −1.5 K for Fe_2 and $Fe_{2.5}$ alloys, respectively. The magnetocaloric properties found revealed the potential of Fe-containing $Ni_{41}Co_9Mn_{40}Sn_{10}$ alloys as room-temperature magnetic refrigerants.

Author agreement

On behalf all authors, I guarantee the following aspects:

(1) All authors have participated sufficiently in this work to take public responsibility for it
(2) All authors have reviewed the final version of the manuscript and approve it for publication
(3) Neither this manuscript nor one with substantially similar content under our authorship has been published or is being considered for publication elsewhere.

Declaration of competing interest

The authors declare that they have no known competing financial interests or personal relationships that could have appeared to influence the work reported in this paper.

CRediT authorship contribution statement

F. Chen: Conceptualization, Methodology, Investigation, Writing - original draft, Funding acquisition. **J.L. Sánchez Llamazares:** Methodology, Writing - review & editing, Funding acquisition. **C.F. Sánchez-Valdés:** Visualization, Investigation, Funding acquisition. **Fenghua Chen:** Methodology, Investigation, Writing - review & editing, Funding acquisition. **Zongbin Li:** Methodology, Investigation, Writing - review & editing. **Y.X. Tong:** Conceptualization, Writing - review & editing. **L. Li:** Conceptualization, Writing - review & editing.

Acknowledgements

The National Natural Science Foundation of China (51101040 and 51804105), the Fundamental Research Funds for the Central Universities (HEUCFG201836), Scientific and Technological Innovation Projects for Excellent Researchers of Shanxi Province (201805D211042) and SEP-CONACYT, Mexico (research project No. A1-S-37066) supported this work. J.L. Sánchez Llamazares acknowledges the scientific and technical support received from Laboratorio Nacional de Investigaciones en Nanociencias y Nanotecnología (LINAN, IPICYT). C.F. Sanchez-Valdés is grateful to DMCU-UACJ for supporting his research stays at IPICYT (program PFCE and academic mobility grant).

References

[1] A.M. Tishin, Y.I. Spichkin, The Magnetocaloric Effect and its Applications, Institute of Physics Publishing, Bristol, 2003.
[2] R. Kumar, Magnetocaloric effect in cryocooler regenerator materials and its applications, Mater. Today: SAVE Proc. 4 (2017) 5544−5551.
[3] V. Franco, J.S. Blázquez, J.J. Ipus, J.Y. Law, L.M. Moreno-Ramírez, A. Conde, Magnetocaloric effect: from materials research to refrigeration devices, Prog. Mater. Sci. 93 (2018) 112−232.
[4] S.A. Nikitin, A.M. Tishin, P.I. Leontiev, Magnetocaloric effect and pressure influence on dysprosium single crystal magnetization in the range of magnetic phase transition, J. Magn. Magn Mater. 92 (1991) 405−416.
[5] V.K. Pecharsky, K.A. Gschneidner Jr., Giant magnetocaloric effect in $Gd_5Si_2Ge_2$, Phys. Rev. Lett. 78 (1997) 4494−4497.
[6] S.A. Nikitin, A.M. Tishin, Magnetocaloric effect in $HoCo_2$ compound, Cryogenics 31 (1991) 166−167.
[7] K.A. Gschneidner Jr., V.K. Pecharsky, A.O. Tsokol, Recent developments in magnetocaloric material, Reports, Prog. Phys. 68 (2005) 1479−1539.
[8] V. Franco, J.S. Blazquez, B. Ingale, A. Conde, The magnetocaloric effect and magnetic refrigeration near room temperature: materials and models, Annu. Rev. Mater. Res. 42 (2012) 305−342.
[9] Y. Zhang, D. Guo, S. Geng, X. Lu, G. Wilde, Structure, magnetic and cryogenic magneto-caloric properties in intermetallic gallium compounds RE_2Co_2Ga (RE = Dy, Ho, Er, and Tm), J. Appl. Phys. 124 (2018), 043903.
[10] D. Guo, H. Li, Y. Zhang, Magnetic phase transition and magnetocaloric effect in ternary Er_2Ni_2Ga compound, IEEE Trans. Magn. 55 (2019) 1−4.
[11] L.W. Li, Review of magnetic properties and magnetocaloric effect in the intermetallic compounds of rare earth with low boiling point metals, Chin. Phys. B 25 (2016), 037502.
[12] Y. Zhang, Review of the structural, magnetic and magnetocaloric properties in ternary rare earth RE_2T_2X type intermetallic compounds, J. Alloys Compd. 787 (2019) 1173−1186.
[13] Y. Zhang, D. Guo, B. Wu, H. Wang, R. Guan, X. Li, Z. Ren, Magnetic properties

and magneto-caloric performances in $RECo_2B_2C$ (RE = Gd, Tb and Dy) compounds, J. Alloys Compd. 817 (2020), 152780.
[14] L. Li, M. Yan, Recent progresses in exploring the rare earth based intermetallic compounds for cryogenic magnetic refrigeration, J. Alloys Compd. (2020), 153810.
[15] F.X. Hu, B.G. Shen, J.R. Sun, Magnetic entropy change involving martensitic transition in NiMn-based Heusler alloys, Chin. Phys. B 22 (2013), 037505.
[16] V. Chaudhary, X. Chen, R.V. Ramanujan, Iron and manganese based magnetocaloric materials for near room temperature thermal management, Prog. Mater. Sci. 100 (2019) 64–98.
[17] A. Smaïli, R. Chahine, Composite materials for Ericsson-like magnetic refrigeration cycle, J. Appl. Phys. 81 (1997) 824–829.
[18] L. Li, Y. Yuan, Y. Qi, Q. Wang, S. Zhou, Achievement of a table-like magnetocaloric effect in the dual-phase $ErZn_2$/ErZn composite, Mater. Res. Lett. 6 (2017) 67–71.
[19] X.C. Zhong, X.Y. Shen, H.Y. Mo, D.L. Jiao, Z.W. Liu, W.Q. Qiu, H. Zhang, R.V. Ramanujan, Table-like magnetocaloric effect and large refrigerant capacity in $Gd_{65}Mn_{25}Si_{10}$ -Gd composite materials for near room temperature refrigeration, Mater. Today Commun. 14 (2018) 22–26.
[20] L. Zhou, Y. Tang, Y. Chen, H. Guo, W. Pang, X. Zhao, Table-like magnetocaloric effect and large refrigerant capacity of composite magnetic refrigerants based on $LaFe_{11.6}Si_{1.4}H_y$ alloys, J. Rare Earths 36 (2018) 613–618.
[21] J. Lyubina, Magnetocaloric materials for energy efficient cooling, J. Phys. D Appl. Phys. 50 (2017), 053002.
[22] L. Li, C. Xu, Y. Yuan, S. Zhou, Large refrigerant capacity induced by table-like magnetocaloric effect in amorphous $Er_{0.2}Gd_{0.2}Ho_{0.2}Co_{0.2}Cu_{0.2}$ ribbons, Mater. Res. Lett. 6 (2018) 413–418.
[23] Y. Zhang, D. Guo, H. Li, S. Geng, J. Wang, X. Li, H. Xu, Z. Ren, G. Wilde, Low field induced large magnetic entropy change in the amorphousized $Tm_{60}Co_{20}Ni_{20}$ ribbon, J. Alloys Compd. 733 (2018) 40–44.
[24] Y. Zhang, H. Li, S. Geng, X. Lu, G. Wilde, Microstructure and cryogenic magnetic properties in amorphousized $RE_{57}Cu_{25}Al_{18}$ (RE = Ho and Tm) ribbons, J. Alloys Compd. 770 (2019) 849–853.
[25] V.K. Pecharsky, A.P. Holm, K.A. Gschneidner Jr., R. Rink, Massive magnetic-field-induced structural transformation in Gd_5Ge_4 and the nature of the giant magnetocaloric effect, Phys. Rev. Lett. 91 (2003), 197204.
[26] E. Brück, H. Yibole, L. Zhang, A universal metric for ferroic energy materials, Phil. Trans. A 374 (2016).
[27] J. Lai, X. You, I. Dugulan, B. Huang, J. Liu, M. Maschek, L. van Eijck, N. van Dijk, E. Brück, Tuning the magneto-elastic transition of $(Mn,Fe,V)_2(P,Si)$ alloys to low magnetic field applications, J. Alloys Compd. 821 (2020), 153451.
[28] L.M. Moreno-Ramírez, C. Romero-Muñiz, J.Y. Law, V. Franco, A. Conde, I.A. Radulov, F. Maccari, K.P. Skokov, O. Gutfleisch, Tunable first order transition in $La(Fe,Cr,Si)_{13}$ compounds: retaining magnetocaloric response despite a magnetic moment reduction, Acta Mater. 175 (2019) 406–414.
[29] N.T. Trung, L. Zhang, L. Caron, K.H.J. Buschow, E. Brück, Giant magnetocaloric effects by tailoring the phase transitions, Appl. Phys. Lett. 96 (2010), 172504.
[30] E. Liu, W. Wang, L. Feng, W. Zhu, G. Li, J. Chen, H. Zhang, G. Wu, C. Jiang, H. Xu, F. de Boer, Stable magnetostructural coupling with tunable magneto-responsive effects in hexagonal ferromagnets, Nat. Commun. 3 (2012), 873.
[31] T. Samanta, P. Lloveras, A.U. Saleheen, D.L. Lepkowski, E. Kramer, I. Dubenko, P.W. Adams, D.P. Young, M. Barrio, J.L. Tamarit, N. Ali, S. Stadler, Barocaloric and magnetocaloric effects in $(MnNiSi)_{1-x}(FeCoGe)_x$, Appl. Phys. Lett. 112 (2018), 021907.
[32] J. Liu, Y. Gong, Y. You, X. You, B. Huang, X. Miao, G. Xu, F. Xu, E. Brück, Giant reversible magnetocaloric effect in MnNiGe-based materials: minimizing thermal hysteresis via crystallographic compatibility modulation, Acta Mater. 174 (2019) 450–458.
[33] A. Biswas, A.K. Pathak, N.A. Zarkevich, X. Liu, Y. Mudryk, V. Balema, D.D. Johnson, V.K. Pecharsky, Designed materials with the giant magnetocaloric effect near room temperature, Acta Mater. 180 (2019) 341–348.
[34] T. Krenke, E. Duman, M. Acet, E.F. Wassermann, X. Moya, L. Mañosa, A. Planes, Inverse magnetocaloric effect in ferromagnetic Ni–Mn–Sn alloys, Nat. Mater. 4 (2005) 450–454.
[35] I. Babita, S.I. Patil, S. Ram, First order structural transformation and inverse magnetocaloric effect in melt-spun Ni–Mn–Sn ribbons, J. Phys. D Appl. Phys. 43 (2010), 205002.
[36] V.V. Khovaylo, K.P. Skokov, O. Gutfleisch, H. Miki, T. Takagi, T. Kanomata, V.V. Koledov, V.G. Shavrov, G. Wang, E. Palacios, J. Bartolomé, R. Burriel, Peculiarities of the magnetocaloric properties in Ni-Mn-Sn ferromagnetic shape memory alloys, Phys. Rev. B 81 (2010), 214406.
[37] T. Krenke, E. Duman, M. Acet, X. Moya, L. Mañosa, A. Planes, Effect of Co and Fe on the inverse magnetocaloric properties of Ni-Mn-Sn, J. Appl. Phys. 102 (2007), 033903.
[38] Z.D. Han, D.H. Wang, B. Qian, J.F. Feng, X.F. Jiang, Y.W. Du, Phase transitions, magnetocaloric effect and magnetoresistance in Ni–Co–Mn–Sn ferromagnetic shape memory alloy, Jpn. J. Appl. Phys. 49 (2010), 010211.
[39] J. Du, Q. Zheng, W.J. Ren, W.J. Feng, X.G. Liu, Z.D. Zhang, Magnetocaloric effect and magnetic-field-induced shape recovery effect at room temperature in ferromagnetic Heusler alloy Ni–Mn–Sb, J. Phys. D Appl. Phys. 40 (2007) 5523–5526.
[40] M. Khan, N. Ali, S. Stadler, Inverse magnetocaloric effect in ferromagnetic $Ni_{50}Mn_{37+x}Sb_{13-x}$ Heusler alloys, J. Appl. Phys. 101 (2007), 053919.
[41] A.K. Nayak, K.G. Suresh, A.K. Nigam, Giant inverse magnetocaloric effect near room temperature in Co substituted NiMnSb Heusler alloys, J. Phys. D Appl. Phys. 42 (2008), 035009.
[42] J. Liu, N. Scheerbaum, J. Lyubina, O. Gutfleisch, Reversibility of magneto-structural transition and associated magnetocaloric effect in Ni–Mn–In–Co, Appl. Phys. Lett. 93 (2008), 102512.
[43] L. Mañosa, D. González-Alonso, A. Planes, E. Bonnot, M. Barrio, J.L. Tamarit, S. Aksoy, M. Acet, Giant solid-state barocaloric effect in the NiMnIn magnetic shape memory alloy, Nat. Mater. 9 (2010) 478–481.
[44] V.K. Sharma, M.K. Chattopadhyay, L.S. Sharath Chandra, S.B. Roy, Elevating the temperature regime of the large magnetocaloric effect in a Ni–Mn–In alloy towards room temperature, J. Phys. D Appl. Phys. 44 (2011), 145002.
[45] J. Liu, T. Gottschall, K.P. Skokov, J.D. Moore, O. Gutfleisch, Giant magnetocaloric effect driven by structural transitions, Nat. Mater. 11 (2012) 620–626.
[46] S. Kavita, V.V. Ramakrishna, P. Yadav, S. Kethavath, N.P. Lalla, T. Thomas, P. Bhatt, R. Gopalan, Enhancement of martensite transition temperature and inverse magnetocaloric effect in $Ni_{43}Mn_{47}Sn_{11}$ alloy with B doping, J. Alloys Compd. 795 (2019) 519–527.
[47] J.Y. Law, Á. Díaz-García, L.M. Moreno-Ramírez, V. Franco, A. Conde, A.K. Giri, How concurrent thermomagnetic transitions can affect magnetocaloric effect: the $Ni_{49+x}Mn_{36-x}In_{15}$ Heusler alloy case, Acta Mater. 166 (2019) 459–465.
[48] Y. Qu, A. Gràcia-Condal, L. Mañosa, A. Planes, D. Cong, Z. Nie, Y. Ren, Y. Wang, Outstanding caloric performances for energy-efficient multicaloric cooling in a Ni-Mn-based multifunctional alloy, Acta Mater. 177 (2019) 46–55.
[49] S.C. Ma, H.C. Xuan, C.L. Zhang, L.Y. Wang, Q.Q. Cao, D.H. Wang, Y.W. Du, Effects of pre-deformation on the martensitic transformation and magnetocaloric property in Ni-Mn-Co-Sn ribbons, Chin. Phys. B 19 (2010), 117503.
[50] S.C. Ma, Q.Q. Cao, H.C. Xuan, C.L. Zhang, L.J. Shen, D.H. Wang, Y.W. Du, Magnetic and magnetocaloric properties in melt-spun and annealed $Ni_{42.7}Mn_{40.8}Co_{5.2}Sn_{11.3}$ ribbons, J. Alloys Compd. 509 (2011) 1111–1114.
[51] A. Ghosh, K. Mandal, Large magnetoresistance associated with large inverse magnetocaloric effect in Ni-Co-Mn-Sn alloys, Eur. Phys. J. B 86 (2013) 378.
[52] L. Huang, D.Y. Cong, H.L. Suo, Y.D. Wang, Giant magnetic refrigeration capacity near room temperature in $Ni_{40}Co_{10}Mn_{40}Sn_{10}$ multifunctional alloy, Appl. Phys. Lett. 104 (2014), 132407.
[53] F. Chen, W.L. Liu, Y.G. Shi, P. Müllner, Influence of annealing on martensitic transformation and magnetic entropy change in $Ni_{37.7}Co_{12.7}Mn_{40.8}Sn_{8.8}$ magnetic shape memory alloy ribbon, J. Magn. Magn Mater. 377 (2015) 137–141.
[54] S.C. Ma, C.W. Shih, J. Liu, J.H. Yuan, S.Y. Lee, Y.I. Lee, H.W. Chang, W.C. Chang, Wheel speed-dependent martensitic transformation and magnetocaloric effect in Ni–Co–Mn–Sn ferromagnetic shape memory alloy ribbons, Acta Mater. 90 (2015) 292–302.
[55] F. Chen, J.L. Sánchez Llamazares, C.F. Sánchez-Valdés, P. Müllner, Y.G. Shi, Y.X. Tong, L. Li, High temperature martensitic transformation and giant magnetocaloric effect in $Ni_{40}Co_{10}Mn_{41}Sn_9$ melt-spun ribbons, J. Alloys Compd. 744 (2018) 493–501.
[56] Y.H. Qu, D.Y. Cong, X.M. Sun, Z.H. Nie, W.Y. Gui, R.G. Li, Y. Ren, Y.D. Wang, Giant and reversible room-temperature magnetocaloric effect in Ti-doped Ni-Co-Mn-Sn magnetic shape memory alloys, Acta Mater. 134 (2017) 236–248.
[57] R. Kainuma, K. Oikawa, W. Ito, Y. Sutou, T. Kanomata, K. Ishida, Metamagnetic shape memory effect in NiMn-based Heusler-type alloys, J. Mater. Chem. 18 (2008), 1837.
[58] F. Chen, J.L. Sánchez Llamazares, C.F. Sánchez-Valdés, F.H. Chen, Y.X. Tong, L. Li, Ni-Co-Mn-Sn quaternary alloys: magnetic hysteresis loss reduction and ductility enhancement by iron alloying, J. Magn. Magn Mater. 485 (2019) 351–357.
[59] A. Quintana-Nedelcos, J.L. Sánchez Llamazares, C.F. Sánchez-Valdés, P. Álvarez Alonso, P. Gorria, P. Shamba, N.A. Morley, On the correct estimation of the magnetic entropy change across the magneto-structural transition from the Maxwell relation: study of MnCoGeBx alloy ribbons, J. Alloys Compd. 694 (2017) 1189–1195.
[60] Y. Feng, J.H. Sui, Z.Y. Gao, J. Zhang, W. Cai, Investigation on martensitic transformation behavior, microstructures and mechanical properties of Fe-doped Ni–Mn–In alloys, Mater. Sci. Eng., A 507 (2009) 174–178.
[61] Z.H. Liu, M. Zhang, W.Q. Wang, W.H. Wang, J.L. Chen, G.H. Wu, F.B. Meng, H.Y. Liu, B.D. Liu, J.P. Qu, Y.X. Li, Magnetic properties and martensitic transformation in quaternary Heusler alloy of NiMnFeGa, J. Appl. Phys. 92 (2002) 5006–5010.
[62] Z. Wu, Z. Liu, H. Yang, Y. Liu, G. Wu, R.C. Woodward, Metallurgical origin of the effect of Fe doping on the martensitic and magnetic transformation behaviours of $Ni_{50}Mn_{40-x}Sn_{10}Fe_x$ magnetic shape memory alloys, Intermetallics 19 (2011) 445–452.
[63] J. Liu, T.G. Woodcock, N. Scheerbaum, O. Gutfleisch, Influence of annealing on magnetic field-induced structural transformation and magnetocaloric effect in Ni–Mn–In–Co ribbons, Acta Mater. 57 (2009) 4911–4920.
[64] R. Kainuma, Y. Imano, W. Ito, Y. Sutou, H. Morito, S. Okamoto, O. Kitakami, K. Oikawa, A. Fujita, T. Kanomata, K. Ishida, Magnetic-field-induced shape recovery by reverse phase transformation, Nature 439 (2006) 957–960.
[65] R. Kainuma, Y. Imano, W. Ito, H. Morito, Y. Sutou, K. Oikawa, A. Fujita, K. Ishida, S. Okamoto, O. Kitakami, T. Kanomata, Metamagnetic shape memory effect in a Heusler-type $Ni_{43}Co_7Mn_{39}Sn_{11}$ polycrystalline alloy, Appl. Phys. Lett. 88 (2006), 192513.
[66] V.K. Pecharsky, K.A. Gschneidner Jr., A.O. Pecharsky, A.M. Tishin, Thermodynamics of the magnetocaloric effect, Phys. Rev. B 64 (2001).
[67] V. Recarte, J.I. Pérez-Landazábal, S. Kustov, E. Cesari, Entropy change linked to the magnetic field induced martensitic transformation in a Ni–Mn–In–Co

shape memory alloy, J. Appl. Phys. 107 (2010), 053501.
[68] E.C. Passamani, F. Xavier, E. Favre-Nicolin, C. Larica, A.Y. Takeuchi, I.L. Castro, J.R. Proveti, Magnetic properties of NiMn-based Heusler alloys influenced by Fe atoms replacing Mn, J. Appl. Phys. 105 (2009), 033919.
[69] C.O. Aguilar-Ortiz, D. Soto-Parra, P. Álvarez-Alonso, P. Lázpita, D. Salazar, P.O. Castillo-Villa, H. Flores-Zúñiga, V.A. Chernenko, Influence of Fe doping and magnetic field on martensitic transition in Ni−Mn−Sn melt-spun ribbons, Acta Mater. 107 (2016) 9−16.
[70] H. Zhang, M. Qian, X. Zhang, L. Wei, F. Cao, D. Xing, X. Cui, J. Sun, L. Geng, Martensite transformation and magnetic properties of Fe-doped Ni-Mn-Sn alloys with dual phases, J. Alloys Compd. 689 (2016) 481−488.
[71] W. Ito, X. Xu, R.Y. Umetsu, T. Kanomata, K. Ishida, R. Kainuma, Concentration dependence of magnetic moment in $Ni_{50-x}Co_xMn_{50-y}Z_y$ (Z=In,Sn) Heusler alloys, Appl. Phys. Lett. 97 (2010), 242512.
[72] H.S. Liu, C.L. Zhang, Z.D. Han, H.C. Xuan, D.H. Wang, Y.W. Du, The effect of Co doping on the magnetic entropy changes in $Ni_{44-x}Co_xMn_{45}Sn_{11}$ alloys, J. Alloys Compd. 467 (2009) 27−30.
[73] T. Krenke, E. Duman, M. Acet, X. Moya, L. Mañosa, A. Planes, Effect of Co and Fe on the inverse magnetocaloric properties of Ni-Mn-Sn, J. Appl. Phys. 102 (2007), 033903.
[74] H.E. Karaca, I. Karaman, B. Basaran, Y. Ren, Y.I. Chumlyakov, H.J. Maier, Magnetic field-induced phase transformation in NiMnCoIn magnetic shape-memory alloys-A new actuation mechanism with large work output, Adv. Funct. Mater. 19 (2009) 983−998.
[75] K. Koyama, K. Watanabe, T. Kanomata, R. Kainuma, K. Oikawa, K. Ishida, Observation of field-induced reverse transformation in ferromagnetic shape memory alloy $Ni_{50}Mn_{36}Sn_{14}$, Appl. Phys. Lett. 88 (2006), 132505.
[76] F. Chen, Y.X. Tong, L. Li, J.L. Sánchez Llamazares, C.F. Sánchez-Valdés, P. Müllner, The effect of step-like martensitic transformation on the magnetic entropy change of $Ni_{40.6}Co_{8.5}Mn_{40.9}Sn_{10}$ unidirectional crystal grown with the Bridgman-Stockbarger technique, J. Alloys Compd. 691 (2017) 269−274.
[77] Z. Li, Z. Li, J. Yang, B. Yang, X. Zhao, L. Zuo, Large room temperature adiabatic temperature variation in a $Ni_{40}Co_8Mn_{42}Sn_{10}$ polycrystalline alloy, Intermetallics 100 (2018) 57−62.
[78] F. Cheng, L. Gao, Y. Wang, J. Wang, X. Liao, S. Yang, Large refrigeration capacity in a $Ni_{42}Co_8Mn_{37.7}In_{12.3}$ magnetocaloric alloy, J. Magn. Magn Mater. 478 (2019) 234−238.
[79] K.A. Gschneidner Jr., V.K. Pecharsky, A.O. Pecharsky, C.B. Zimm, Mater. Sci. Forum 315−317 (1999) 69.
[80] M.E. Wood, W.H. Potter, General analysis of magnetic refrigeration and its optimization using a new concept: maximization of refrigerant capacity, Cryogenics 25 (1985) 667−683.
[81] J. Ren, H.W. Li, J.K. Yu, S.T. Feng, Q.J. Zhai, J.X. Fu, Z.P. Luo, H.X. Zheng, Enhanced magnetocaloric effect in Heusler Ni−Mn−Sn unidirectional crystal, J. Alloys Compd. 634 (2015) 65−69.
[82] A.G. Varzaneh, P. Kameli, T. Amiri, K.K. Ramachandran, A. Mar, I.A. Sarsari, J.L. Luo, T.H. Etsell, H. Salamati, Effect of Cu substitution on magnetocaloric and critical behavior in $Ni_{47}Mn_{40}Sn_{13-x}Cu_x$ alloys, J. Alloys Compd. 708 (2017) 34−42.
[83] T.L. Phan, P. Zhang, N.H. Dan, N.H. Yen, P.T. Thanh, T.D. Thanh, M.H. Phan, S.C. Yu, Coexistence of conventional and inverse magnetocaloric effects and critical behaviors in $Ni_{50}Mn_{50-x}Sn_x$ (x = 13 and 14) alloy ribbons, Appl. Phys. Lett. 101 (2012), 212403.
[84] L. Huang, D.Y. Cong, L. Ma, Z.H. Nie, Z.L. Wang, H.L. Suo, Y. Ren, Y.D. Wang, Large reversible magnetocaloric effect in a Ni-Co-Mn-In magnetic shape memory alloy, Appl. Phys. Lett. 108 (2016), 032405.
[85] A. Taubel, T. Gottschall, M. Fries, S. Riegg, C. Soon, K.P. Skokov, O. Gutfleisch, A comparative study on the magnetocaloric properties of Ni-Mn-X(-Co) Heusler alloys, Phys. Status Solidi 255 (2018), 1700331.
[86] F. Chen, Y.X. Tong, L. Li, J.L. Sánchez Llamazares, C.F. Sánchez-Valdés, P. Müllner, Broad first-order magnetic entropy change curve in directionally solidified polycrystalline Ni-Co-Mn-In, J. Alloys Compd. 727 (2017) 603−609.
[87] X. Zhang, H. Zhang, M. Qian, L. Geng, Enhanced magnetocaloric effect in Ni-Mn-Sn-Co alloys with two successive magnetostructural transformations, Sci. Rep. 8 (2018), 8235.
[88] T. Paramanik, I. Das, Near room temperature giant magnetocaloric effect and giant negative magnetoresistance in Co, Ga substituted Ni−Mn−In Heusler alloy, J. Alloys Compd. 654 (2016) 399−403.
[89] X. Wang, F. Sun, J. Wang, Q. Yu, Y. Wu, H. Hua, C. Jiang, Influence of annealing temperatures on the magnetostructural transition and magnetocaloric effect of $Ni_{40}Co_{10}Mn_{40}Sn_{10}$ powders, J. Alloys Compd. 691 (2017) 215−219.
[90] H. Zhang, X. Zhang, M. Qian, L. Wei, D. Xing, J. Sun, L. Geng, Enhanced magnetocaloric effects of Ni-Fe-Mn-Sn alloys involving strong metamagnetic behavior, J. Alloys Compd. 715 (2017) 206−213.
[91] Y. Zhang, J. Liu, Q. Zheng, J. Zhang, W.X. Xia, J. Du, A. Yan, Large magnetic entropy change and enhanced mechanical properties of Ni−Mn−Sn−C alloys, Scripta Mater. 75 (2014) 26−29.
[92] J. Brock, M. Khan, Large refrigeration capacities near room temperature in $Ni_2Mn_{1-x}Cr_xIn$, J. Magn. Magn Mater. 425 (2017) 1−5.
[93] S. Pandey, A. Quetz, A. Aryal, I. Dubenko, D. Mazumdar, S. Stadler, N. Ali, Magnetocaloric, thermal, and magnetotransport properties of $Ni_{50}Mn_{35}In_{13.9}B_{1.1}$ Heusler alloy, J. Magn. Magn Mater. 444 (2017) 98−101.
[94] Z. Li, S. Dong, Z. Li, B. Yang, F. Liu, C.F. Sánchez-Valdés, J.L. Sánchez Llamazares, Y. Zhang, C. Esling, X. Zhao, L. Zuo, Giant low-field magnetocaloric effect in Si alloyed Ni-Co-Mn-In alloys, Scripta Mater. 159 (2019) 113−118.
[95] J. Yan, Z.Z. Li, X. Chen, K.W. Zhou, S.X. Shen, H.B. Zhou, Martensitic transition and magnetocaloric properties in $Ni_{45}Mn_{44-x}Fe_xSn_{11}$ alloys, J. Alloys Compd. 506 (2010) 516−519.
[96] A. Wójcik, W. Maziarz, M.J. Szczerba, M. Sikora, A. Żywczak, C.O. Aguilar-Ortiz, P. Álvarez-Alonso, E. Villa, H. Flores-Zúñiga, E. Cesari, J. Dutkiewicz, V.A. Chernenko, Transformation behavior and inverse caloric effects in magnetic shape memory $Ni_{44-x}Cu_xCo_6Mn_{39}Sn_{11}$ ribbons, J. Alloys Compd. 721 (2017) 172−181.
[97] A. Ghosh, K. Mandal, Effect of structural disorder on the magnetocaloric properties of Ni-Mn-Sn alloy, Appl. Phys. Lett. 104 (2014), 031905.